The 2MASS Redshift Survey in the Zone of Avoidance

Lucas M. Macri,[1] Renée C. Kraan-Korteweg,[2] Trystan Lambert,[3] María Victoria Alonso,[4,5] Perry Berlind,[6]
Michael Calkins,[6] Pirin Erdoğdu,[7] Emilio E. Falco,[6] Thomas H. Jarrett,[2] and Jessica D. Mink[6]

[1]*George P. & Cynthia Woods Mitchell Institute for Fundamental Physics and Astronomy, Department of Physics & Astronomy,
Texas A&M University, 4242 TAMU, College Station, TX 77843-4242, USA*
[2]*Department of Astronomy, University of Cape Town, Private Bag X3, Rondebosch 7701, South Africa*
[3]*South African Astronomical Observatory, PO Box 9, Observatory 7935, Cape Town, South Africa*
[4]*Instituto de Astronomía Teórica y Experimental (IATE-CONICET), Laprida 854, X5000BGR Córdoba, Argentina*
[5]*Observatorio Astronómico de Córdoba Universidad Nacional de Córdoba, Córdoba, Argentina*
[6]*Harvard-Smithsonian Center for Astrophysics, 60 Garden St, Cambridge, MA 02138, USA*
[7]*Department of Physics and Astronomy, University College London, Gower St, London WC1E 6BT, UK*

ABSTRACT

The 2MASS Redshift Survey was started two decades ago with the goal of mapping the three-dimensional distribution of an all-sky flux-limited ($K_s < 11.75$ mag) sample of $\sim 45,000$ galaxies. Our first data release (Huchra et al. 2012) presented an unprecedented uniform coverage for most of the celestial sphere, with redshifts for $\sim 98\%$ of our sample. However, we were missing redshifts for $\sim 18\%$ of the catalog entries that were located within the "Zone of Avoidance" ($|b| < 10°$) – an important region of the sky for studies of large-scale structure and cosmic flows.

In this second and final data release, we present redshifts for all 1,041 2MRS galaxies that previously lacked this information, as well as updated measurements for 27 others.

Keywords: galaxies: distances and redshifts — cosmology: large-scale structure of universe — catalogs

1. INTRODUCTION

Decades of concerted efforts have yet to resolve the tension between local cosmic flows and cosmology: what gives rise to our peculiar motion, and is it consistent with ΛCDM? Answering these question requires knowledge of the local cosmography (based on the observed distribution of luminous matter) and the peculiar velocity field (which originates from the combined distribution of both luminous and dark matter). The persistent discrepancies in the derived Local Group motion are thought to be due to incomplete mapping of large-scale structures at low Galactic latitudes, in the so-called "Zone of Avoidance" (ZoA; Kraan-Korteweg & Lahav 2000; Loeb & Narayan 2008).

Obtaining a complete redshift sample in the ZoA is crucial for this endeavor. This area of the sky contains some of the largest mass concentrations in the local Universe, such as the core of the Great Attractor (Kraan-Korteweg et al. 1996), the Pisces-Perseus Supercluster (Ramatsoku et al. 2014, 2016), and the recently-discovered Vela Supercluster (Kraan-Korteweg et al. 2017). This latest discovery highlights the importance of spectroscopic surveys for finding and mapping additional large mass concentrations.

Our understanding of the large-scale structures and associated dynamics in the nearby Universe is increasingly being refined thanks to the advances of larger and more systematic redshift surveys. The Two Micron All-Sky Survey (2MASS) produced an "extended source catalog" with $\sim 1.5 \times 10^6$ galaxies complete to $K_S = 13.5$ (Jarrett et al. 2000). The 2MASS Redshift Survey (2MRS: Huchra et al. 2005) was started two decades ago with the goal of obtaining redshifts for all of the $\sim 45,000$ brightest 2MASS galaxies ($K_s < 11.75$, extinction-corrected) outside of the innermost ZoA (defined as $|b| < 8°$ for $-30° < l < 30°$ and $|b| < 5°$ otherwise).
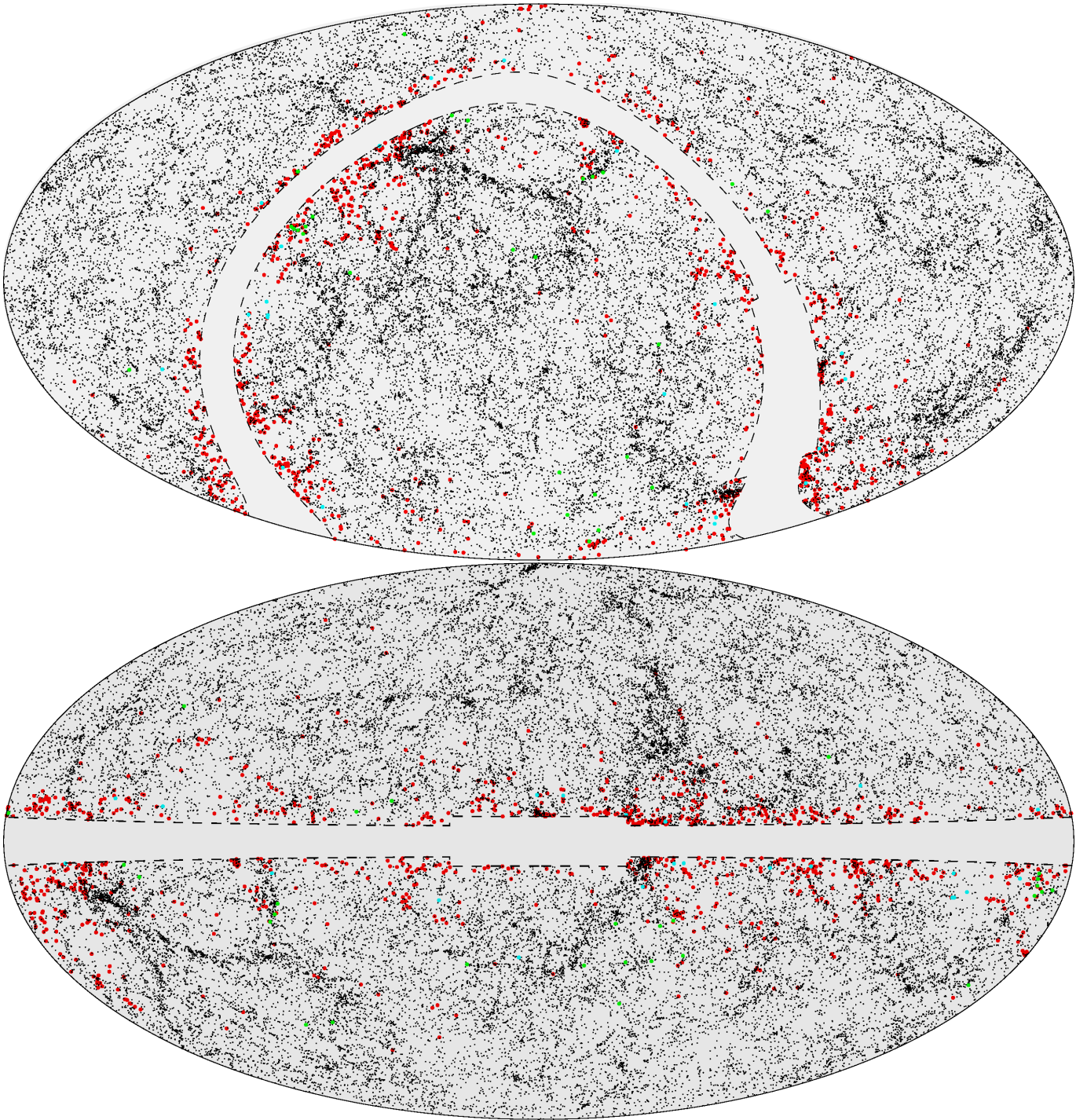
Corresponding author: Lucas M. Macri
lmacri@tamu.edu

Figure 1. All-sky distribution of 2MRS galaxies in equatorial (top) and Galactic (bottom) coordinates. These Aitoff projections are centered at (α, δ) and (l, b) of $(0, 0)$ with the longitudinal coordinate increasing to the left. Black dots: galaxies with redshifts presented in H12; red dots: galaxies without redshifts in H12, presented here for the first time; green dots: galaxies with redshifts in H12 that have been updated; cyan dots: entries removed from the catalog (mistakenly classified as galaxies). Dashed lines indicate the boundaries of 2MRS ($|b| < 8°$ for $-30° < l < 30°$; $|b| < 5°$ otherwise).

Our initial data release (Huchra et al. 2012, hereafter H12) presented measurements for 97.6% of the sample, including new observations of 11,000 galaxies with previously unknown redshifts. 2MRS has been (and continues to be) extensively used for studies of the large-scale structure (Jarrett 2004), group and clustering properties (Crook et al. 2007, T. Lambert et al., in preparation), the dipole motion (Erdoğdu et al. 2006a), and the local density and velocity fields (Erdoğdu et al. 2006b; Heß & Kitaura 2016). The 2MASS Tully-Fisher survey (2MTF; Masters et al. 2008) obtained high-quality 21-cm linewidths for 493 2MRS galaxies which, combined with measurements from the literature, have yielded a catalog of 2062 distances based on the Tully-Fisher relation (Tully & Fisher 1977) and corresponding peculiar velocities (Hong et al. 2019). Among other applications, 2MTF has been used to study the velocity power spectrum (Howlett et al. 2017) and to determine the bulk flow out to $D \sim 40$ Mpc (Hong et al. 2019). These efforts are complementary to those of the 6dFGS project (Jones et al. 2009), which obtained redshifts for a deeper ($K_s \lesssim 12.5$ mag) sample of 2MASS galaxies (but was limited to the Southern hemisphere) and used the fundamental plane of elliptical galaxies (Dressler et al. 1987) to derive distances (Magoulas et al. 2012).

2. OBSERVATIONS

Our previous data release (H12) consisted of 43,533 and 1,066 galaxies with and without redshifts, respectively. During the course of our observations, we identified 26 objects in the latter set that were removed from the catalog; these were stars, badly-centered duplicates of other galaxies already in the catalog, or star/galaxy blends that severely compromised the photometry of the extended source. Additionally, we removed one galaxy from the set with redshifts, which was a badly-centered duplicate of an object present in the set without redshifts. The existing redshift measurement was reassigned to the latter. After these changes, the 2MRS catalog consists of 44,572 galaxies (please refer to Table A1 for details of all changes relative to H12). Fig. 1 shows the all-sky distribution of 2MRS sources in equatorial and Galactic coordinates.

We noticed that two galaxies ($08533956 + 7256532$ and $17564915 - 8156263$) had been erroneously assigned redshifts in H12 so they were moved to the set without redshifts, which consisted of 1,041 targets after all the aforementioned changes. One of us (R.K.K.) contributed previously-unpublished measurements for 39 objects and we found redshifts in NED (NASA/IPAC Extragalactic Database) for five galaxies (Crook et al.

2007; Guzzo et al. 2009; Schröder et al. 2009), leaving 997 objects to be observed.

Given the relatively bright apparent magnitudes ($V \lesssim 16$ mag) and the low density of our targets in the sky (~ 1 per sq. deg.), observations of these objects are most efficiently carried out using medium-aperture ($2 - 4$ m) telescopes with long-slit spectrographs. We used the following facilities between 2012 May and 2018 September to obtain 1,023 redshifts (for the 997 aforementioned targets and for repeat observations of 26 galaxies with redshifts in H12, mainly due to very large uncertainties in the previous measurements):

- The Tillinghast 1.5-m telescope at the Fred L. Whipple Observatory (FLWO) with the "FAst Spectrograph for the Tillinghast" (FAST; Fabricant et al. 1998) yielded 573 redshifts (code "F" on Table 1).

- The Radcliffe 1.9-m telescope at the South African Astronomical Observatory (SAAO) with the CassSpec and "Spectrograph Upgrade: Newly Improved Cassegrain" (SpUpNIC) spectrographs (Crause et al. 2019) yielded 403 redshifts (code "Z" on Table 1).

- The Jorge Sahade 2.2-m telescope at the Complejo Astronómico El Leoncito (CASLEO) with the REOSC spectrograph (Baume et al. 2017) yielded 37 redshifts (code "L" on Table 1).

- The Southern Astrophysical Research (SOAR) 4.1-m telescope at the Cerro Tololo Interamerican Observatory with the Goodman spectrograph Clemens et al. (2004) yielded 8 redshifts (code "G" on Table 1).

- The Hiltner 2.4-m telescope at the Michigan-Dartmouth-MIT (MDM) observatory with the Ohio State Multi-Object Spectrograph (OSMOS; Martini et al. 2011) yielded 2 redshifts (code "M" on Table 1).

3. ANALYSIS AND RESULTS

All spectra were analyzed following the same procedures described in detail in §3.2 of H12. Our measurements have been corrected to the barycentric reference frame, and all corrections were applied using the proper product of $(1 + z)$ factors. We chose to express our redshifts in units of cz, noting that the IRAF RVSAO package used in our analysis adopted $c = 299,792.5$ km/s. As pointed out by Davis et al. (2019, and references therein), further analyses of our data and other redshift
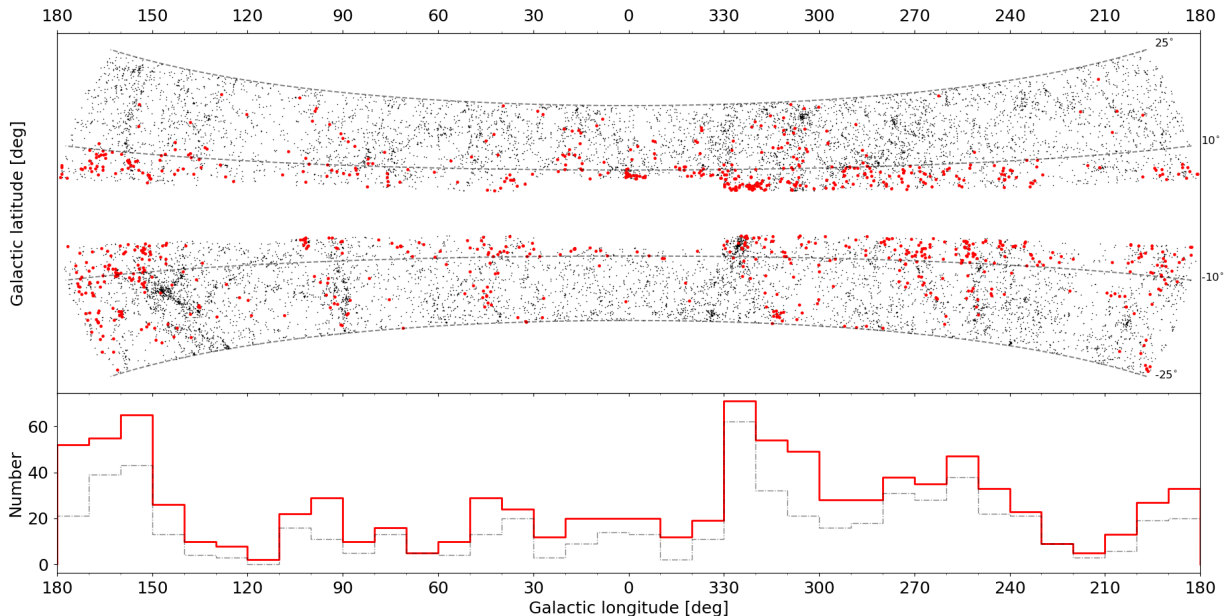
Figure 2. Distribution of the 1,068 new redshifts that complete 2MRS. Top: zoom of Fig. 1b, focusing on $|b| \leq 25°$; red dots (marginally enlarged for visibility) represent the new redshifts, while black dots show the galaxies from H12. Bottom: histogram of the new redshifts as function of Galactic longitude for $|b| \leq 25°$ (red line) and the inner ZOA $|b| \leq 10°$ (dashed grey line).

surveys should always be done in units of z to avoid various systematic biases. This is especially important for peculiar velocity studies. The median statistical uncertainty of the redshifts was $c\sigma(z) = 41$ km/s. We estimated the systematic uncertainty of our measurements by making repeated observations of several bright galaxies that serve as radial velocity standards (N1316, N1365, N1404, N5846, N7552) and comparing our error-weighted mean redshifts with reference values[1]. We found a negligible $c\langle\Delta z\rangle = 4 \pm 14$ km/s, consistent with our typical statistical uncertainty of 23 km/s for these objects.

Table 1 presents our results, following the same format and layout as Table 3 of H12. The columns are described in detail in the table footnote and in the machine-readable version available online. There are 1,068 entries (997 new observations, 39 previously-unpublished measurements, 26 reobserved galaxies, 5 measurements from the literature, and 1 object replaced).

The overall 2.4% incompleteness in redshifts from H12 was far from uniform across the sky. It was heavily biased toward the ZoA, where many prominent nearby large-scale structures are located: the Great Attractor, the Perseus-Pisces and Ophiuchus superclusters, and the Local Void (among others). The incompleteness in H12 increased from 6.3% at $|b| < 25°$ to 17.8% at $|b| < 10°$,

leaving many of the aforementioned features poorly sampled at low Galactic latitudes. This was due to the inherent difficulties of getting good-quality spectra for galaxies affected by increased dust extinction and higher stellar density and sky brightness levels. Even along the Galactic equator the new redshifts are inhomogeneously distributed.

This is illustrated in Fig. 2, with the top panel zoomed into the ZoA and the bottom panel displaying histograms of the new 2MRS observations as a function of Galactic longitude; 90% (57%) of these measurements are contained within $|b| = 25°$ (10°). Many (but not all) of the clumps in new redshifts are associated with known large-scale structure features. This could well be of relevance to the aforementioned studies of the dipole motion and local flow fields, and to studies of group properties, such as those presented in our companion paper (Lambert et al. 2019).

In the following, we provide some insight into some of these new features which are also apparent in Fig. 3 and Fig. 4. The former shows the all-sky 2MRS galaxy distribution in Galactic coordinates, color-coded for redshift, where the color-coding is closely matches H12. Note how neatly the completed 2MRS lines up with its nominal latitude boundaries compared to the more ragged delineation in H12 around $|b| = 5°$. The latter displays the distribution of 2MRS galaxies in various projections of the SuperGalactic plane.
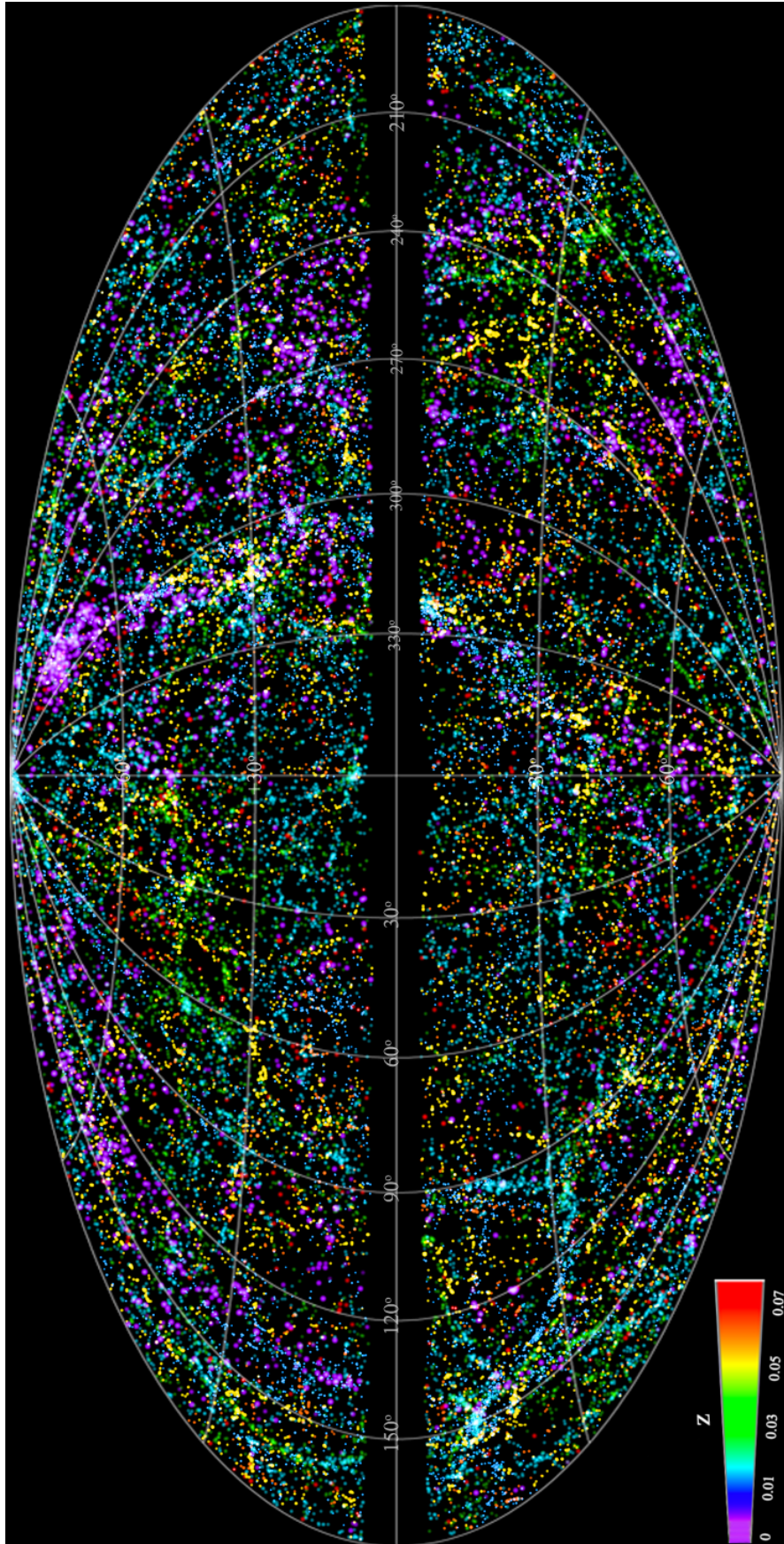
Figure 3. All-sky distribution of 2MRS galaxies in Galactic coordinates, using color to convey their redshifts. Completeness in the ZoA (relative to H12) yields a tighter delination of the survey boundaries.
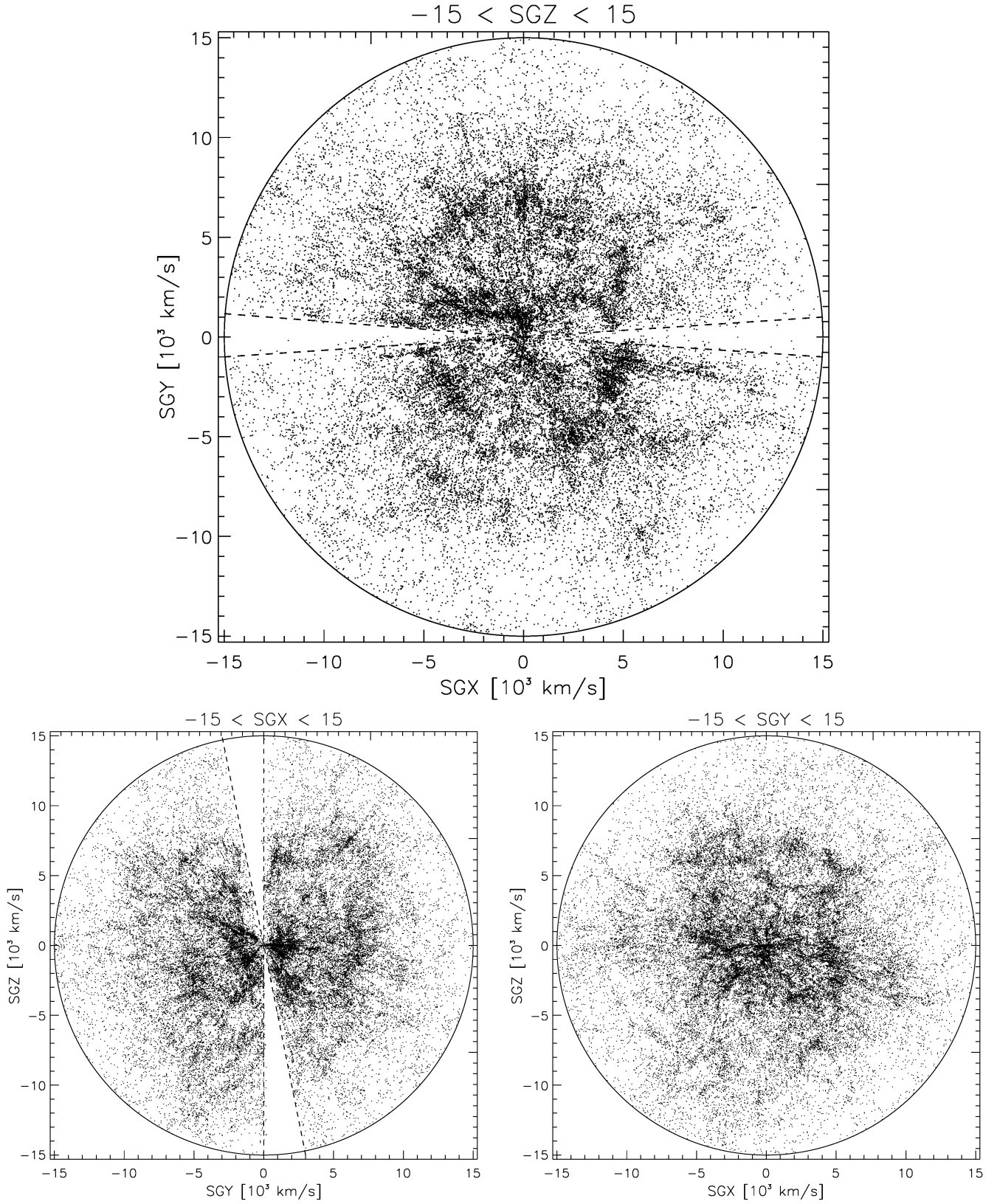
Figure 4. Distribution of 2MRS galaxies in SuperGalactic coordinates, using units of 10^3 km/s. Top: projection into the (SGX,SGY) plane; bottom left: projection into the (SGY,SGZ) plane; bottom right: projection into the (SGX,SGZ) plane. The approximate boundaries of our survey due to the innermost ZoA are shown using dashed lines.

Table 1. 2MRS Catalog (columns 1-13)

(1)	(2)	(3)	(4)	(5)	(6)	(7)	(8)	(9)	(10)	(11)	(12)	(13)
2MASS ID	R.A.	Dec.	l	b	K_s^0	H^0	J^0	$K_{s,t}^0$	H_t^0	J_t^0	$\sigma(K_s^0)$	$\sigma(H^0)$
	(deg)		(deg)		(mag)							
$02485298 + 5302143$	42.22079	53.03735	140.17172	-5.85763	9.537	9.726	10.426	9.445	9.632	10.341	0.030	0.024
$04270415 + 2027093$	66.76727	20.45259	176.31357	-19.38375	9.883	10.093	10.758	9.799	9.993	10.671	0.036	0.029
$05384231 + 1544532$	84.67630	15.74814	190.44562	-8.25286	9.928	10.136	10.787	9.848	10.057	10.708	0.037	0.024
$09463018 - 2134178$	146.62576	-21.57161	255.66951	23.88194	10.101	10.358	11.044	10.000	10.251	10.931	0.048	0.035
$19121580 - 6358361$	288.06598	-63.97664	332.13776	-26.43528	10.272	10.558	11.220	10.021	10.009	10.678	0.054	0.044
$12525011 - 1018361$	193.20883	-10.31006	303.49725	52.56010	10.410	10.676	11.359	10.305	10.436	11.168	0.046	0.028
$03212772 + 4048059$	50.36548	40.80168	151.24796	-13.67875	10.462	10.723	11.401	10.267	10.485	11.152	0.045	0.036
$04194441 + 3557293$	64.93507	35.95812	163.36200	-10.07978	10.618	10.896	11.647	10.521	10.790	11.529	0.046	0.038
$06074593 + 3225063$	91.94147	32.41850	179.36438	5.86340	10.692	10.944	11.627	10.534	10.850	11.523	0.045	0.044
$05430236 + 1620591$	85.75992	16.34973	190.46982	-7.05045	10.723	10.951	11.632	10.604	10.801	11.490	0.051	0.030
$05174145 + 1936010$	79.42268	19.60033	184.42633	-10.39923	10.726	11.122	11.994	10.629	10.989	11.887	0.050	0.036
$06010670 + 3342353$	90.27802	33.70980	177.55162	5.26711	10.819	11.247	12.304	10.733	11.135	12.164	0.044	0.047
$05323561 + 1522511$	83.14842	15.38087	189.98283	-9.69933	10.841	11.155	11.843	10.691	11.008	11.694	0.061	0.038
$18570768 - 7828212$	284.28232	-78.47256	315.86765	-26.82081	10.841	11.444	12.261	10.825	11.237	11.943	0.050	0.052
$04301670 + 2326448$	67.56960	23.44573	174.42603	-16.87470	10.857	11.029	11.807	10.698	10.819	11.617	0.063	0.039
$05242105 + 1422371$	81.08781	14.37709	189.77205	-11.91985	10.905	11.138	11.841	10.816	11.069	11.796	0.056	0.033
$05232510 + 1633198$	80.85459	16.55557	187.77589	-10.93586	10.916	11.113	11.789	10.823	11.010	11.705	0.062	0.035
$17413903 - 0437191$	265.41263	-4.62198	20.59406	13.25158	10.970	11.223	11.972	10.714	10.943	11.717	0.052	0.045
$08324123 - 5113345$	128.17188	-51.22622	268.17825	-6.73042	10.995	11.237	12.090	10.776	11.035	11.920	0.069	0.051
$07365795 - 4047484$	114.24139	-40.79684	254.12871	-9.49531	11.005	11.153	11.870	10.886	10.960	11.604	0.070	0.041
$07244714 + 1405193$	111.19660	14.08878	203.90164	13.66018	11.031	11.368	12.270	10.968	11.152	12.082	0.039	0.030
$18044513 + 1731392$	271.18802	17.52752	43.84589	17.99977	11.102	11.377	12.122	10.922	11.194	11.956	0.057	0.042
$05272524 + 1612051$	81.85517	16.20144	188.60564	-10.31789	11.107	11.403	12.143	11.019	11.311	12.080	0.059	0.036
$20595692 - 5533431$	314.98718	-55.56196	341.67456	-40.07023	11.121	11.324	11.908	10.919	11.111	11.734	0.083	0.055
$14593308 - 5154213$	224.88797	-51.90596	322.14438	6.12193	11.123	11.367	12.108	10.687	11.359	11.769	0.090	0.077
$23122811 - 6131165$	348.11710	-61.52133	321.77420	-51.83395	11.123	11.450	12.069	11.038	11.348	11.944	0.058	0.044

NOTE—This table is presented in its entirety in the online version of the paper.

Table 1. 2MRS Catalog (columns 14-26)

(1)	(14)	(15)	(16)	(17)	(18)	(19)	(20)	(21)	(22)	(23)	(24)	(25)	(26)
2MASS ID	$\sigma(J^0)$	$\sigma(K_t^0)$	$\sigma(H_t^0)$	$\sigma(J_t^0)$	E_{BV}	$r_{\rm iso}$	$r_{\rm ext}$	b/a	flags	Type	t_src	cz	$c\sigma(z)$
		(mag)			(mag)	$(\log_{10} '')$						(km/s)	
$02485298+5302143$	0.020	0.029	0.024	0.022	0.493	1.615	1.776	0.420	0111	3	ZC	4735	25
$04270415+2027093$	0.023	0.033	0.026	0.026	0.576	1.529	1.702	0.460	0000	0X	ZC	3856	21
$05384231+1544532$	0.021	0.034	0.022	0.022	0.518	1.504	1.680	0.560	0000	98	NN	5234	26
$09463018-2134178$	0.024	0.046	0.032	0.027	0.047	1.444	1.634	0.780	0666	0	JH	8794	31
$19121580-6358361$	0.030	0.047	0.031	0.023	0.041	1.455	1.664	0.500	0000	0	JH	11045	44
$12525011-1018361$	0.021	0.046	0.027	0.028	0.041	1.449	1.692	0.300	0333	4	JH	4096	18
$03212772+4048059$	0.026	0.043	0.035	0.033	0.149	1.330	1.604	0.720	0331	-2	ZC	6088	21
$04194441+3557293$	0.030	0.042	0.038	0.034	0.588	1.356	1.556	0.420	0333	3	ZC	5248	22
$06074593+3225063$	0.033	0.040	0.045	0.039	0.715	1.398	1.617	0.500	0000	98	NN	8608	42
$05430236+1620591$	0.024	0.044	0.029	0.026	0.485	1.303	1.512	0.620	0000	98	NN	5737	27
$05174145+1936010$	0.035	0.046	0.039	0.040	0.580	1.520	1.695	0.180	0133	2	ZC	5272	40
$06010670+3342353$	0.053	0.046	0.049	0.062	0.799	1.394	1.596	0.220	0000	98	NN	7698	28
$05323561+1522511$	0.036	0.052	0.038	0.039	0.641	1.338	1.543	0.640	0000	98	NN	6402	11
$18570768-7828212$	0.038	0.058	0.059	0.044	0.156	1.161	1.502	0.560	0000	0B	JH	12977	46
$04301670+2326448$	0.036	0.056	0.038	0.040	0.900	1.297	1.526	0.600	0333	5	JH	5424	44
$05242105+1422371$	0.029	0.049	0.034	0.033	0.419	1.356	1.557	0.360	0444	2	ZC	5882	23
$05232510+1633198$	0.030	0.054	0.035	0.040	0.403	1.332	1.537	0.520	0000	0X	ZC	5710	36
$17413903-0437191$	0.044	0.080	0.066	0.066	0.717	1.422	1.707	0.500	0111	7	ZC	7962	14
$08324123-5113345$	0.056	0.064	0.056	0.072	0.960	1.243	1.526	0.720	0000	98	NN	11521	84
$07365795-4047484$	0.037	0.064	0.039	0.037	0.672	1.179	1.419	0.720	0333	98	NN	8725	57
$07244714+1405193$	0.027	0.036	0.028	0.030	0.126	1.017	1.301	0.960	0333	4	JH	5405	29
$18044513+1731392$	0.031	0.051	0.045	0.037	0.120	1.281	1.542	0.540	0333	-1	JH	5544	16
$05272524+1612051$	0.036	0.055	0.038	0.043	0.615	1.318	1.525	0.420	0111	2	ZC	5721	33
$20595692-5533431$	0.036	0.070	0.054	0.038	0.049	1.428	1.638	0.440	0000	0	JH	2003	23
$14593308-5154213$	0.074	0.114	0.166	0.130	0.584	1.270	1.708	0.780	0222	98	NN	11102	32
$23122811-6131165$	0.029	0.053	0.045	0.032	0.018	1.204	1.439	0.880	0000	-2	JH	7884	29

NOTE—This table is presented in its entirety in the online version of the paper.

Table 1. 2MRS Catalog (columns 27-29)

(1)	(27)	(28)	(29)
2MASS ID	cat	v_src	Catalog ID
02485298 + 5302143	F	20192MRS.FLWO.0000M	02485298+5302143
04270415 + 2027093	F	20192MRS.FLWO.0000M	04270415+2027093
05384231 + 1544532	F	20192MRS.FLWO.0000M	05384231+1544532
09463018 − 2134178	Z	20192MRS.SAAO.0000M	09463018-2134178
19121580 − 6358361	Z	20192MRS.SAAO.0000M	19121580-6358361
12525011 − 1018361	L	20192MRS.CSLO.0000M	12525011-1018361
03212772 + 4048059	F	20192MRS.FLWO.0000M	03212772+4048059
04194441 + 3557293	F	20192MRS.FLWO.0000M	04194441+3557293
06074593 + 3225063	F	20192MRS.FLWO.0000M	06074593+3225063
05430236 + 1620591	F	20192MRS.FLWO.0000M	05430236+1620591
05174145 + 1936010	F	20192MRS.FLWO.0000M	05174145+1936010
06010670 + 3342353	F	20192MRS.FLWO.0000M	06010670+3342353
05323561 + 1522511	F	20192MRS.FLWO.0000M	05323561+1522511
18570768 − 7828212	Z	20192MRS.SAAO.0000M	18570768-7828212
04301670 + 2326448	F	20192MRS.FLWO.0000M	04301670+2326448
05242105 + 1422371	F	20192MRS.FLWO.0000M	05242105+1422371
05232510 + 1633198	F	20192MRS.FLWO.0000M	05232510+1633198
17413903 − 0437191	F	20192MRS.FLWO.0000M	17413903-0437191
08324123 − 5113345	L	20192MRS.CSLO.0000M	08324123-5113345
07365795 − 4047484	L	20192MRS.CSLO.0000M	07365795-4047484
07244714 + 1405193	L	20192MRS.CSLO.0000M	07244714+1405193
18044513 + 1731392	F	20192MRS.FLWO.0000M	18044513+1731392
05272524 + 1612051	L	20192MRS.CSLO.0000M	05272524+1612051
20595692 − 5533431	Z	20192MRS.SAAO.0000M	20595692-5533431
14593308 − 5154213	Z	20192MRS.SAAO.0000M	14593308-5154213
23122811 − 6131165	Z	20192MRS.SAAO.0000M	23122811-6131165

NOTE—This table is presented in its entirety in the online version of the paper. Codes for column 27 that identify our new observations are: [F], FLWO/FAST; [G], SOAR/Goodman; [L], CASLEO/REOSC; [M], MDM/OSMOS; [Z], SAAO/CassSpec or SpUpNIC. [N] denotes redshifts from NED (NASA/ADS bibliographic code given in column 28). [2], [6], [K], [O], [P], [S] refer to previously unpublished observations by RKK (see online table for details).

In the Perseus-Pisces complex (PP; $150° < l < 200°$) a filamentary extension from Perseus ($l \sim 150°$) toward the Galactic Plane around 165° shows up quite prominently for the first time. The feature connects to a ridge in the ZoA, which encompasses the 3C 129 cluster that links PP to Lynx (see Ramatsoku et al. 2016; Kraan-Korteweg et al. 2018). It also traces the continuation of the second PP arm ($l \sim 90°$) closer to the ZoA, connecting to a filamentary extension across the ZoA found with H I observations (Kraan-Korteweg et al. 2018). The concentration around $l \sim 100°, b \sim -5°$ (seen in green in Fig. 3) is a complete surprise, seemingly forming an isolated group or small cluster around 12,000 km/s. The clump of redshifts at $l \sim 0°, b \sim +5°$ (seen in cyan in Fig. 3) is centered around 10,000 km/s and hence clearly part of the Ophiuchus supercluster (Wakamatsu et al. 2005).

The number of new redshifts in the general direction of the Great Attractor (GA; $l = 320° - 330°$) is also quite high. While quite a few of the new redshifts are at the GA distance and are partly linked to the Norma cluster (Woudt et al. 2008), the majority actually peak around 12-16,000 km/s and are, therefore, more likely to be associated with the overdensity encompassing the Ara and TriAus clusters in that region. Two further clumps around $l = 250°$ and 270° also rise up in the histogram of Fig 2, both with a high concentration of galaxies around 12-13,000 km/s. The latter also has a significant number of galaxies that lie around 18-20,000 km/s and thus seems to form part of the Vela supercluster (Kraan-Korteweg et al. 2017).

REFERENCES

Baume, G., Coronel, C., De Bórtoli, B., et al. 2017, Boletin de la Asociacion Argentina de Astronomia La Plata Argentina, 59, 46

Clemens, J. C., Crain, J. A., & Anderson, R. 2004, in Proc. SPIE, Vol. 5492, Ground-based Instrumentation for Astronomy, ed. A. F. M. Moorwood & M. Iye, 331–340

Crause, L. A., Gilbank, D., van Gend, C., et al. 2019, JATIS, 5, 024007, doi: 10.1117/1.JATIS.5.2.024007

Crook, A. C., Huchra, J. P., Martimbeau, N., et al. 2007, ApJ, 655, 790, doi: 10.1086/510201

Davis, T. M., Hinton, S. R., Howlett, C., & Calcino, J. 2019, MNRAS, 490, 2948, doi: 10.1093/mnras/stz2652

Dressler, A., Lynden-Bell, D., Burstein, D., et al. 1987, ApJ, 313, 42, doi: 10.1086/164947

Erdoğdu, P., Huchra, J. P., Lahav, O., et al. 2006a, MNRAS, 368, 1515, doi: 10.1111/j.1365-2966.2006.10243.x

Erdoğdu, P., Lahav, O., Huchra, J. P., et al. 2006b, MNRAS, 373, 45, doi: 10.1111/j.1365-2966.2006.11049.x

Fabricant, D., Cheimets, P., Caldwell, N., & Geary, J. 1998, PASP, 110, 79, doi: 10.1086/316111

Guzzo, L., Schuecker, P., Böhringer, H., et al. 2009, A&A, 499, 357, doi: 10.1051/0004-6361/200810838

Heß, S., & Kitaura, F.-S. 2016, MNRAS, 456, 4247, doi: 10.1093/mnras/stv2928

Hong, T., Staveley-Smith, L., Masters, K. L., et al. 2019, MNRAS, 487, 2061, doi: 10.1093/mnras/stz1413

Howlett, C., Staveley-Smith, L., Elahi, P. J., et al. 2017, MNRAS, 471, 3135, doi: 10.1093/mnras/stx1521

Huchra, J., Martimbeau, N., Jarrett, T., et al. 2005, in IAU Symposium, Vol. 216, Maps of the Cosmos, ed. M. Colless, L. Staveley-Smith, & R. A. Stathakis, 170

Huchra, J. P., Macri, L. M., Masters, K. L., et al. 2012, ApJS, 199, 26, doi: 10.1088/0067-0049/199/2/26

Jarrett, T. 2004, PASA, 21, 396, doi: 10.1071/AS04050

Jarrett, T. H., Chester, T., Cutri, R., et al. 2000, AJ, 119, 2498, doi: 10.1086/301330

Jones, D. H., Read, M. A., Saunders, W., et al. 2009, MNRAS, 399, 683, doi: 10.1111/j.1365-2966.2009.15338.x

Kraan-Korteweg, R. C., Cluver, M. E., Bilicki, M., et al. 2017, MNRAS, 466, L29, doi: 10.1093/mnrasl/slw229

Kraan-Korteweg, R. C., & Lahav, O. 2000, A&A Rv, 10, 211, doi: 10.1007/s001590000011

Kraan-Korteweg, R. C., van Driel, W., Schröder, A. C., Ramatsoku, M., & Henning, P. A. 2018, MNRAS, 481, 1262, doi: 10.1093/mnras/sty2285

Kraan-Korteweg, R. C., Woudt, P. A., Cayatte, V., et al. 1996, Nature, 379, 519, doi: 10.1038/379519a0

Lambert, T., Kraan-Korteweg, R. C., Jarrett, T. H., & Macri, L. M. 2019, in preparation

Loeb, A., & Narayan, R. 2008, MNRAS, 386, 2221, doi: 10.1111/j.1365-2966.2008.13187.x

Magoulas, C., Springob, C. M., Colless, M., et al. 2012, MNRAS, 427, 245, doi: 10.1111/j.1365-2966.2012.21421.x

Martini, P., Stoll, R., Derwent, M. A., et al. 2011, PASP, 123, 187, doi: 10.1086/658357

Masters, K. L., Springob, C. M., & Huchra, J. P. 2008, AJ, 135, 1738, doi: 10.1088/0004-6256/135/5/1738

Ramatsoku, M., Kraan-Korteweg, R., Schröder, A., & van Driel, W. 2014, in SAIP2012: the 57th Annual Conference of the South African Institute of Physics, ed. J. van Rensburg, 368–372

Ramatsoku, M., Verheijen, M. A. W., Kraan-Korteweg, R. C., et al. 2016, MNRAS, 460, 923, doi: 10.1093/mnras/stw968

Schröder, A. C., Kraan-Korteweg, R. C., & Henning, P. A. 2009, A&A, 505, 1049, doi: 10.1051/0004-6361/200912592

Tully, R. B., & Fisher, J. R. 1977, A&A, 54, 661

Wakamatsu, K., Malkan, M. A., Nishida, M. T., et al. 2005, in Astronomical Society of the Pacific Conference Series, Vol. 329, Nearby Large-Scale Structures and the Zone of Avoidance, ed. A. P. Fairall & P. A. Woudt, 189

Woudt, P. A., Kraan-Korteweg, R. C., Lucey, J., Fairall, A. P., & Moore, S. A. W. 2008, MNRAS, 383, 445, doi: 10.1111/j.1365-2966.2007.12571.x

APPENDIX

A. CHANGES TO THE 2MRS CATALOG

In the table below we list the deletions of entries in the 2MRS catalog, relative to H12. We provide redshifts when available (in some cases, the object was rejected by visual inspection before obtaining a spectrum).

Table A1. Deletions from the 2MRS Catalog

2MASS ID	Reason for deletion
$01515799 + 7126330$	star, $v = -59 \pm 46$
$04253337 + 4201067$	star, $v = -66 \pm 44$
$04304237 + 6347222$	star
$05504348 + 1027466$	star+galaxy, $v = -90 \pm 72$ and $cz = 12232 \pm 78$
$06073397 - 0541583$	star
$06081453 - 0934490$	stsar, $v = 51 \pm 12$
$06091575 - 1011338$	star
$06341666 - 0915552$	star, $v = 126 \pm 12$ (Hα)
$06355814 + 2240350$	duplicate of $06355890 + 2240352$, redshift already in H12
$08290119 - 5121097$	star+galaxy
$09002997 - 2224422$	star+galaxy
$09295260 - 6210339$	duplicate of $09295846 - 6210599$
$13224883 - 5629132$	star+galaxy, $v = -37 \pm 54$
$14201250 - 6821596$	stars
$14302060 - 5355016$	galactic source? WISE W4=2.3 mag
$14522589 - 6711268$	star+galaxy, $v = 371 \pm 43$
$15341907 - 4534416$	star+galaxy, $v = 97 \pm 51$
$15524980 - 4032516$	star+galaxy, $v = 187 \pm 39$
$16123697 - 3629426$	star+galaxy, $v = 36 \pm 47$
$16131380 - 6234545$	star+galaxy, $v = 147 \pm 68$
$16292221 - 2652276$	star
$16523424 - 1959028$	star+galaxy, 6dF $v = -56 \pm 45$
$16584354 - 6629079$	star
$19190956 - 0258564$	star+galaxy, $v = 487 \pm 141$
$20015711 - 0649486$	star+galaxy, $v = -108 \pm 26$ and $cz = 1469 \pm 91$
$20451931 - 3514274$	duplicate of $20451841 - 3514264$
$21504406 + 4159299$	star+galaxy, $v = -183 \pm 55$ and $cz = 5572 \pm 54$